ISSN 1846-6168 (Print), ISSN 1848-5588 (Online)
https://doi.org/10.31803/tg-20250127200641

Original scientific paper
Received: 2025-01-27, Accepted: 2025-03-04

The Influence of Copper Plate Dimensions on Temperature Distribution during TIG Welding

Mihael Zelić*, Matija Bušić, Tomislav Veliki

Abstract: This research investigates the influence of copper plate dimensions on temperature distribution during TIG (Tungsten Inert Gas) welding of Cu-ETP (Electrolytic Tough Pitch Copper). When welding copper and lightly alloyed copper alloys with high thermal conductivities, the appropriate type of current and shielding gas must be selected to ensure sufficient heat input. This high heat input compensates for the rapid heat dissipation and cooling in the localized weld zone. The required heat input is determined by the dimensions of the copper sheets to be welded. Experimental measurements using thermocouples were performed on plates with identical thicknesses but varying dimensions, while numerical simulations via ANSYS complemented the analysis. The results highlight the significant impact of plate dimensions on heat dissipation and temperature gradients, providing valuable insights for improving welding settings.

Keywords: Cu-ETP; heat conduction; numerical simulations; thermal conductivity; TIG welding

1 INTRODUCTION

Copper and copper alloys are widely used in many industrial applications for their high electrical and thermal conductivities, good combinations of strength and ductility, and excellent corrosion resistance [1]. The welding of copper and copper alloys is a critical process in producing various components for the chemical and beverages industry, such as high-voltage power transformers, nuclear waste processing, etc. Copper's exceptional thermal and electrical conductivity makes it widely used, but these properties present significant challenges during welding [2]. Copper's high thermal conductivity rapidly dissipates heat from the welding zone, making it difficult to maintain optimal welding temperatures [2]. Additionally, copper oxidizes quickly at high temperatures, potentially compromising weld quality and causing defects [2].

Copper is not subject to phase transformations and cannot be hardened through heat treatment, a characteristic shared by many of its alloys. This characteristic poses additional challenges in maintaining mechanical strength during welding processes [3]. This challenge is further exacerbated by the fact that thermal exposure induces softening in cold-worked copper alloys, resulting in a pronounced reduction in mechanical strength within the heat-affected zone [3].

TIG welding, which employs a non-consumable tungsten electrode in an inert gas atmosphere, has proven to be an effective method for welding copper [2]. This technique ensures precise heat control and minimal weld contamination, which is critical for achieving high-quality joints with high purity and minimal inclusions. This is particularly important in industries where reliability and durability are paramount [3]. Welding generates substantial heat, significantly influencing the base material's microstructure and mechanical properties [3]. The direction and extent of heat distribution in the welded metal are closely linked to the residual stresses and deformations that develop during the cooling phase. Therefore, predicting heat distribution within the material is essential, especially for optimizing weld quality and mitigating defects.

From a practical standpoint, analytical solutions offer the benefit of exceptional computational speed [4]. However, their limited accuracy often becomes a constraint when applied to complex engineering problems such as welding simulations [4], prompting researchers to explore more refined numerical methods. Consequently, numerous researchers have sought to improve analytical approaches, but these efforts have achieved only marginal gains in precision [5-8]. Numerical solutions, on the other hand, provide a higher degree of accuracy but require substantial computational resources [9].

The finite element method (FEM) was initially applied in welding simulations for static and dynamic analyses and later evolved to tackle more intricate issues involving geometric and material nonlinearities. Early studies, such as those by Ueda and Yamakawa [9] and Hibbit and Marcal [10] in the 1970s, pioneered the integration of thermal and mechanical analyses, addressing large deformations and nonlinear stress conditions. Marcal [11] underscored the exceptional complexity of welding as a nonlinear problem in structural mechanics. Goldak et al. [12] noted that the challenges faced by these pioneers discouraged many experts from entering the field. Despite these obstacles, tools like MARC, developed by Marcal and Hibbit, and ABAQUS, created by Hibbit, emerged as foundational programs for advanced welding simulations, becoming essential for nonlinear analysis.

Over the last 30 years, welding simulations have drawn significant research interest, particularly in addressing complex challenges like copper welding. This focus has led to numerous publications and reviews, such as [11–16], which provide valuable insights into progress and best practices. Notably, Lindgren's extensive reviews [14–16] offer a thorough summary of past studies, the current state of the field, and specific guidelines for modeling welding processes to achieve targeted simulation objectives. These efforts have contributed significantly to advancing the understanding and practical implementation of welding simulations. The aim of this research is to analyze heat input, heat conduction, and temperature distribution during TIG welding of copper plates. The focus will be on examining

temperature distribution across varying dimensions of copper plates, analyzing welding parameters' influence on weld quality, and employing numerical methods to simulate thermal processes. The study will include theoretical analysis, experimental measurements, and simulations to comprehensively understand the process. The experimental component of the study will involve detailed measurements of temperature distribution on copper plates during TIG welding using thermocouples at selected points. Simulations will be conducted using ANSYS to accurately model and compare results, with the collected data being used to optimize welding parameters to achieve the highest weld quality.

2 EXPERIMENT

In this experiment, the temperature as a function of time was measured during heating to simulate the TIG welding process for Copper ETP plates with various dimensions. Measurements were taken at 10 positions on each plate, as illustrated in Fig. 1 below.

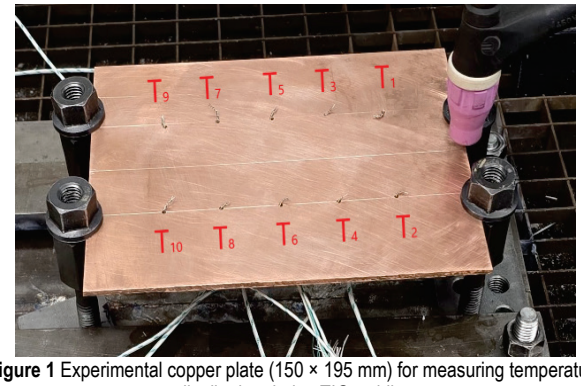

Figure 1 Experimental copper plate (150 × 195 mm) for measuring temperature distribution during TIG welding

The temperature was recorded using K-type thermocouples connected to a precision temperature measurement device (Fluke 1586A Super-DAQ). The test plates featured designated positions (T1, T2, T3, T4, T5, T6, T7, T8, T9, T10) indicating the locations where the thermocouples were fixed, allowing for indirect temperature determination via voltage differences. The experiment used two plates of equal length but different widths (Figs. 2 and 3).

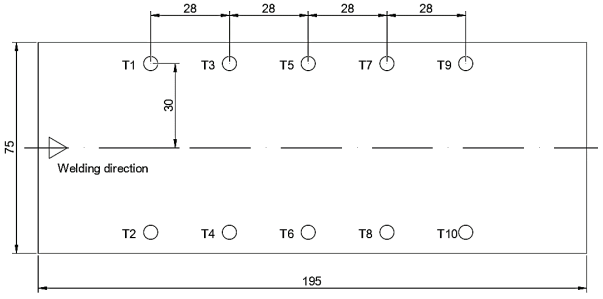

Figure 2 Experimental copper plate (75× 195 mm) for measuring temperature distribution during TIG welding

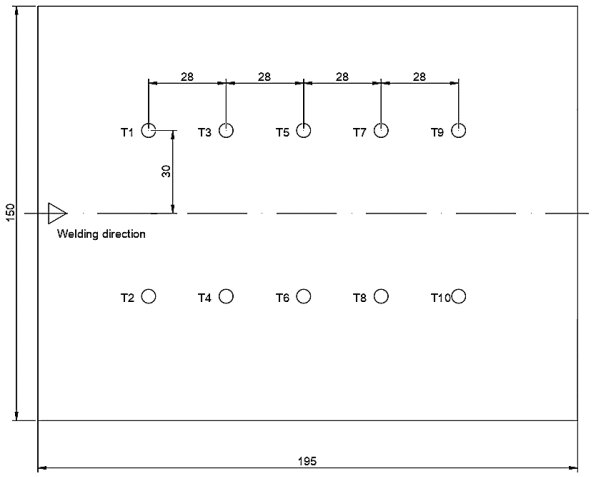

Figure 3 Experimental copper plate (150 × 195 mm) for testing temperature distribution during TIG welding

In both cases, the thermocouples were positioned at an equal distance of 30 mm from the heat input line. The thickness of both plates was identical, measuring 3 mm. The TIG torch was guided using an automated PROMOTECH Rail Bull system.

2.1 Welding Base Material

The plates used in this experiment were made of Cu-ETP copper, in the form of sheets with a thickness of 3 mm and dimensions of 195 × 150 mm and 195 × 75 mm. The material certificate confirms the chemical composition of the Cu-ETP copper used, as listed in Tab. 1 below [17].

Table 1 The material chemical composition [17]

Composition			
Cu	O	Bi	Pb
min 99.9 %	max 0.04 %	max 0.0005 %	max 0.005 %

Tab. 2 provides thermophysical data for the Cu ETP material used in the experiment.

Table 2 Thermophysical data for the Cu ETP [17]

Property of Cu - ETP	Value	Condition
Density, ρ	8.9 g/cm^3	At 20 °C
Thermal Conductivity, k	394 W/m·K	At 20 °C
Specific Heat Capacity, c	0.386 J/g·K	At 20 °C
Emissivity, ε	Up to 0.78	Oxidized Copper
Convective Heat Transfer Coefficient, a_c	5-25 W/m^2·K	Free Convection (Air)

2.2 Experimental Methods and Equipment

The following equipment was used in the experiment:

- Precision Temperature Scanner: Fluke 1586A Super-DAQ, used for accurate temperature measurements and data logging.
- K-Type Thermocouples: Employed for real-time monitoring of temperature distribution on the copper plates.
- TIG Welding Machine: VARTIG 005 AC/DC, providing a stable and controllable heat source for the TIG process.

- Automated Electrode Guiding System: PROMOTECH Rail Bull ensures consistent and precise movement of the welding electrode along the specified welding path.

2.2.1 The Measuring Equipment and Uncertainties

The 1586A Super-DAQ, Fig. 4, is a low voltage 6 ½ digits multimeter that enables precise measurement of temperature and electrical values and, when combined with the internal modules, up to 40 channels can be scanned [18].

Figure 4 Fluke 1586A Super-DAQ, [18]

Measurement was performed with 10 Thermocouple Type K class 1 inserted in their respective holes on the plate and connected to the internal 1586-2586 High-Capacity Modul. Cold Junction Compensation was internal, and the delay time between channels was 0.5 s, enabling scanning at a more accurate medium speed mode. Reading was stored in the internal memory of the multimeter. The uncertainty of the temperature acquisition was in the mentioned setup 0.6 K over the whole range according to the manufacturer specification [18]. Thermocouples were new, unused 0.5 mm Type K from Omega Engineering, mineral fiber insulated, and suitable for measurement up to 1200 °C. Uncertainty of such thermocouples is 1.5 K, according to the [19]. To minimize the uncertainty of the measurement, equipment was calibrated as a temperature indicator (both the thermocouples and the multimeter) according to the [20] in the same configuration as it was to be used for the measurement. Calibration was performed in the range from 30 °C to 350 °C, and the resolution of the reading on the multimeter was 0.01 K. The Thermal source in the range of 30 °C to 150 °C was Druck Premium Calibrator PTC165 [21] with a calibration uncertainty of 0.250 K (K = 2, P = 98 %). All thermocouples were within the range after the stabilization of the thermal source and internal CJC. The range from 200 °C to 350 °C, the Additel 875 Dry Well Calibrator with calibration block was used [22]. Uncertainty of the temperature source was 0.6 K (K = 2, P = 98 %), and again, readings of all thermocouples were within the range. Uncertainty of the thermal zone as determined by the calibration includes stability, radial and axial gradients, and loading effect. The inhomogeneity effect of the thermocouple wire was not considered, as the thermocouples were new and used only for the experiment. Based on the abovementioned uncertainty, the measured temperature in the experiment is estimated to be 0.6 K (K = 2, P = 98 %), and no correction on measured values has been applied.

2.2.2 VARTIG Welding Sources

Vartig welding sources are designed for the TIG process, with the additional capability of welding with coated electrodes. They are suitable for welding structural and stainless steels, aluminum, and copper. The devices feature a digital display of welding parameters and LED indicators for various operating modes [23]. Tab. 3 presents the welding parameters, which were identical for both plates [23].

Table 3 Welding parameters applied in experiments.

Welding parameter	Type/ value
Current type	Direct current (DC)
Electrode polarity	Electrode negative (EN, SP)
Current intensity	120 A
W electrode diameter	3.2 mm
W electrode type	Wla 15
Vertex angle of the W electrode	45 °
Electrode to workpiece angle	90 °
Shielding gas	Argon 4.8
Shielding gas flow rate	12 l/min
Welding position	PA (down hand, flat)
Arc voltage	14.8 V
Welding speed	5.3 mm/s

The gas flow was 12 l/min. Samples were welded using pure argon. This shielding gas, which has the trademark name Argon 4.8 (with a purity of 99,998%), is classified as I1 according to standard EN ISO 14175:2008 [23].

2.2.3 Automated Electrode Guiding Device

The PROMOTECH Rail Bull device, Fig. 5, automates the linear movement of the TIG torch and is designed for TIG-MIG/MAG welding or plasma cutting.

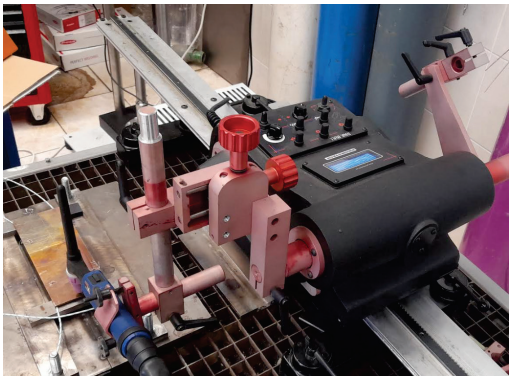

Figure 5 Automated TIG Torch Guiding in the Experiment

The device moves over ferromagnetic and non-ferromagnetic materials using a rack-and-rail drive system. The rails can be attached to flat or curved surfaces using magnetic or vacuum units, with the minimum curvature radius for the semi-flexible track being 5 m [23].

2.3 Results of the Experiment

In Fig. 6, the temperature distributions over time can be seen for a plate with dimensions of 75 × 195 mm, while in Fig. 7, the temperature distribution is shown for a plate with dimensions of 150 × 195 mm.

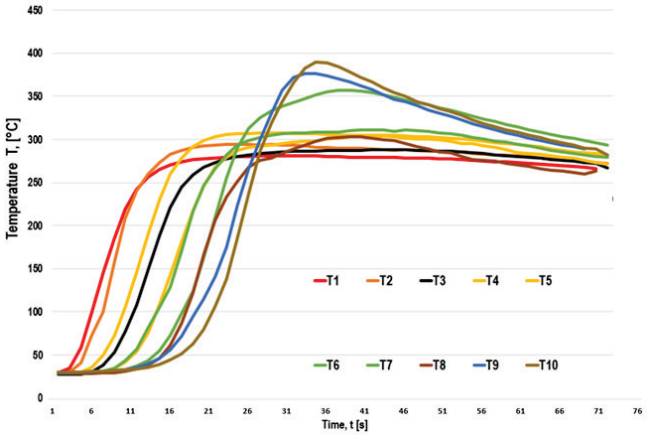

Figure 6 Graph of the plate (75 × 195 mm) temperature dependence on time for the thermocouples

The maximum temperature achieved by the smaller plate is T_{max} = 390 °C, recorded at thermocouple 10. An initial increase in temperature is observed, following an exponential heating pattern, up to the maximum temperature T_{max}, after which a cooling phase occurs with a negative gradient. Differences between the thermocouples indicate an asymmetrical heat distribution, where thermocouples closer to the welding zone record higher values, while those farther away show lower values and take longer to reach the peak temperature. Symmetrical thermocouples should display identical temperatures under ideal conditions, such as in ANSYS simulations. This is expected and can be explained by the fact that the material is not perfect, the thermocouples did not measure at perfectly symmetrical points, and the clamps caused asymmetrical heat dissipation. Fig. 6 shows temperature functions for all thermocouples on the plate with dimensions 75 × 195 mm. However, in the experiment, differing temperatures are observed. They can experience minor geometric misalignments, even on the order of a few millimeters, which lead to localized differences in heat flow. They may also encounter uneven contact with clamps or surface irregularities, as well as material inhomogeneities, creating zones of increased or decreased heat dissipation. They are further influenced by changing environmental conditions, such as airflow and localized radiation, which affect cooling and can introduce measurement variations. Thermocouples T1 and T2 initially exhibit a rapid temperature increase due to a brief yet intense interaction with the heat source, followed by an extended cooling period. In contrast, T9 and T10 require more time to reach elevated temperatures due to slower heat transfer, which leads to higher final temperature readings. Nonetheless, the overall heat balance still indicates that the heat input exceeds its dissipation. Fig. 7 shows the graphs for the plate with dimensions 150 × 195 mm. An almost exponential rise is observed across all thermocouples, culminating in peaks that increase with each subsequent thermocouple. The temperature reaches T_{max} = 180,15 °C at T8, followed by a cooling phase with a negative gradient. All curves descend after T8 reaches this peak, governed by heat dissipation mechanisms (convection, contact with clamps or surroundings, and radiation). In contrast, the smaller 75 × 195 mm plate exhibits a higher peak temperature (up to 390 °C) and faster heating, attributable to its lower thermal mass and smaller surface area. The larger plate distributes the input heat over more material, which results in a reduced maximum temperature, a slower overall heating profile, and an extended cooling period due to increased thermal inertia.

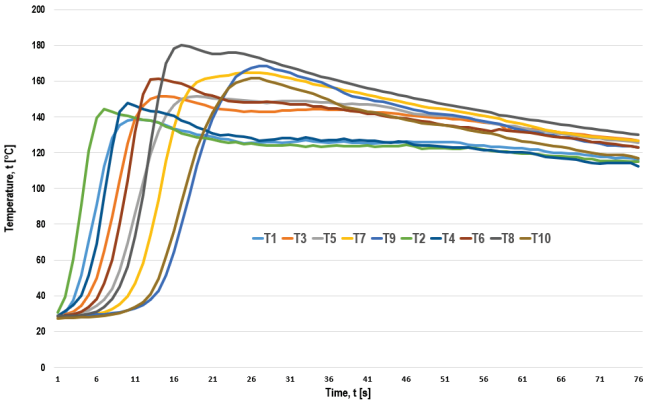

Figure 7 Graph of the plate (150 × 195 mm) temperature dependence on time for the thermocouples

2.4 Effect of Plate Dimensions on Temperature Distribution

Larger plates generally exhibit a greater capacity for heat dissipation due to their increased surface area, which facilitates conduction and radiation. Consequently, temperature gradients across larger plates are less pronounced than those on smaller plates, where heat remains more localized. The geometry of the plate significantly influences heat flow paths. In smaller plates, heat conduction is constrained by the shorter distance to the edges, leading to faster cooling at the boundaries. In contrast, larger plates allow heat to take longer to reach the edges, resulting in a more uniform temperature distribution near the weld line.

Experimental observations revealed notable differences in temperature measurements at symmetrical points on plates of varying dimensions. Smaller plates displayed higher peak temperatures confined closer to the weld zone. In contrast, larger plates demonstrated a broader heat-affected zone with lower peak temperatures, indicating a more dispersed heat distribution. In this paper, plates with dimensions of 75 × 195 mm and 150 × 195 mm are used to more accurately investigate the effect of plate width on heat distribution during TIG welding. By selecting non-standard dimensions, more pronounced temperature gradients and varied cooling rates are achieved, which cannot be accomplished with conventional standard plates. This approach ensures a better correlation between experimental results and numerical simulations, thereby contributing to the optimization of welding parameters.

3 NUMERICAL ANSYS SIMULATION

All four states of matter are present during TIG welding, and their physics is highly complex. The TIG process combines magnetohydrodynamics, plasma physics, and material science [24]. ANSYS uses the finite element method

(FEM) to analyze thermodynamic processes, including transient thermal analysis. This method divides complex geometries into smaller elements for solving heat transfer equations [24]. The simulation analyzed convection, conduction, and heat radiation in the plates, base, and fixators. Phase changes of the molten material and the influence of the latent heat of melting were not considered. Initially, the starting temperature of the plates was defined, along with the heat dissipation coefficients for radiation and convection with the surrounding air. All other thermophysical properties of the material were defined within the simulation (Fig. 8).

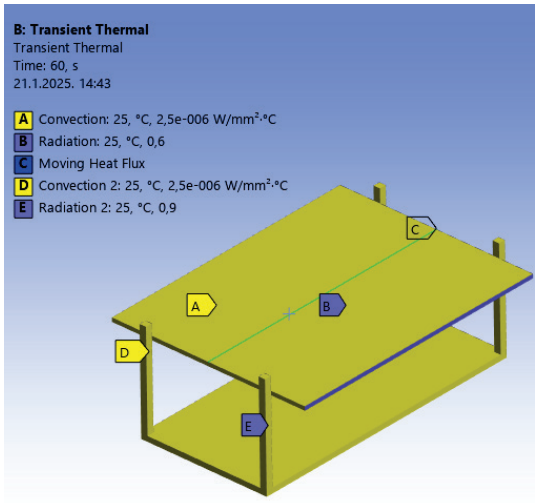

Figure 8 Initial conditions of radiation and heat convection for the measurement setup

3.1 Geometry Model and Meshing

The geometry model in ANSYS was meshed (Fig. 9) using the mechanical physics preference and adaptive sizing.

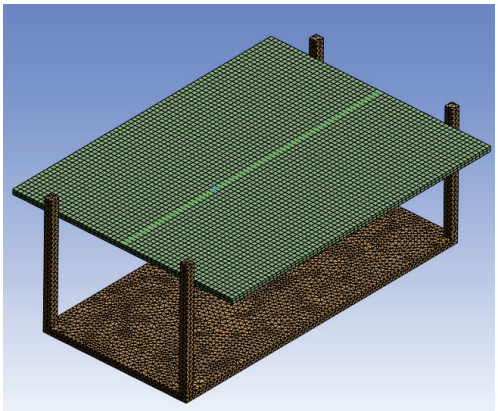

Figure 9 The generated mesh grid in ANSYS

The mesh for the smaller plate consists of 106,927 nodes and 45,535 elements, with a minimum edge length of 2,8 mm. The mesh for the larger plate includes 68,611 nodes and 30,884 elements. The average surface area of the elements was calculated as 4,359.3 mm², with a bounding box diagonal of 266.02 mm.

3.2 Heat Source

Considering that the welding source is relatively far from the temperature distribution measurement location, the source's power distribution is not a relevant factor [24]. Therefore, a simple circular heat source model was used. The source distribution is described as a radial cylinder with a diameter of $r_0 = 5$ mm, as shown in Fig. 10.

The parameters of the welding source are shown in the following Fig. 11. The travel speed is 5.3 mm/s along the plate's symmetry (i.e., along the weld), while the power of the source is 18 W/mm².

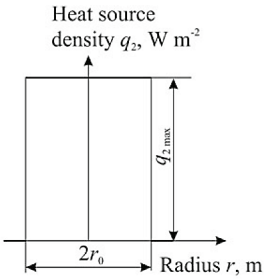

Figure 10 Circular source with constant heat source density q_{arc}, [25]

Details of "Moving Heat Flux"

Geometry	
Scoping Method	Geometry Selection
Geometry	2 Faces
Path	
Scoping Method	Geometry Selection
Geometry	1 Edge
Start Point	
Scoping Method	Geometry Selection
Geometry	1 Vertex
Definition	
Index	1
First Patch?	Yes
Last Patch?	Yes
Velocity	5.3 mm/s
Radius of the Beam	5 mm
Source Power Intensity	18 W/mm²
Start Time	0 s
End Time	37 s
Number of Segments	200
Minimum Steps for Cooling Phase	20
Material Removal	No
Melting Temperature	1080°C

Figure 11 Parameters of the moving heat source

The amount of heat input per unit length of the weld is given by the following Eq. (1) [25]:

$$Q_{\text{net}} = \frac{U \cdot I}{\text{v}} \cdot \eta \tag{1}$$

The variables in the above equation represent the following:

- $U = 14.8$ V, welding voltage
- $I = 120$ A, electric current
- $v = 5.33$ mm/s, welding speed
- $l = 3.2$ mm, arc length
- η heat transfer efficiency coefficient.

Using a nonlinear three-dimensional heat transfer model, a formula for arc efficiency was derived, which can be seen below [25]:

$$\eta = 0.947 - 0.00017 \cdot I - 0.057 \cdot l + 0.02 \cdot v$$
$$\eta = 0.85 \quad (2)$$

The power of the source is then:

$$q_{arc} = U \cdot I \cdot \eta = 14.8 \cdot 120 \cdot 0.85$$
$$q_{arc} = 1509.6 \text{ W} \quad (3)$$

3.3 Boundary Conditions and Heat Equation

The ANSYS simulation solves the thermal partial differential equation over a finite number of elements. At the start of the process, the initial temperature of the workpiece is set to 298.15 K, which is also the ambient temperature. The boundary conditions on the upper surface of the workpiece are defined by the following expression [25]:

$$k\frac{\partial T}{\partial z} = q_{arc} - a_c(T - T_a) - \varepsilon\sigma_B(T^4 - T_a^4) \quad (4)$$

This equation represents the thermal energy balance in the system, where heat conduction $k\frac{\partial T}{\partial z}$ is balanced by the heat input from the arc source q_{arc}, the heat loss due to convection $-a_c(T - T_a)$, and the heat loss due to radiation $-\varepsilon\sigma_B(T^4 - T_a^4)$.

Where: a_c - the heat transfer coefficient between the material and air (W/m^2·K); T_a - the air temperature (K); ε - the material's emissivity factor; σ_b - the Boltzmann constant, 5.67×10^{-8} (W/m^2·K^4); k - thermal conductivity of the material (W/m·K).

The boundary conditions at the edges of the model are expressed by the following equation [25]:

$$k\frac{\partial T}{\partial z} = -a_c(T - T_a) - \varepsilon\sigma_B(T^4 - T_a^4) \quad (5)$$

4 RESULTS OF ANSYS SIMULATION AND DISCUSSION

Fig. 12 shows the temperature distribution from the ANSYS simulation at a specific moment during welding for a plate with dimensions of 75 × 195 mm. The maximum measured temperature on the smaller plate is T_{max} = 728.93 °C, while on the larger plate, the maximum temperature is predictably lower, at T_{max} = 610.45 °C. As stated, the temperature was measured in thermal probes at the exact locations where the temperature was measured using thermocouples in the experiment.

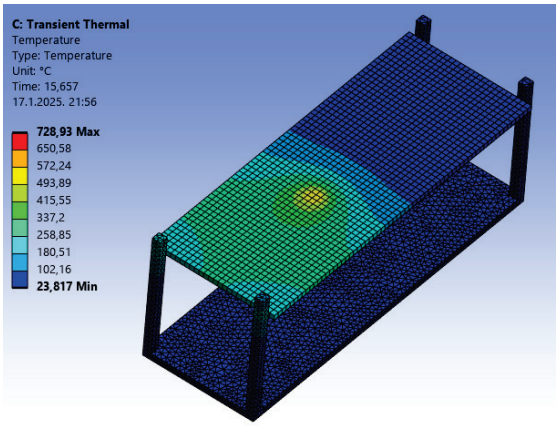

Figure 12 Temperature distribution in a 75 × 195 mm plate welding simulation

In contrast, Fig. 13 also displays the temperature distribution for a plate with 150 × 195 mm dimensions.

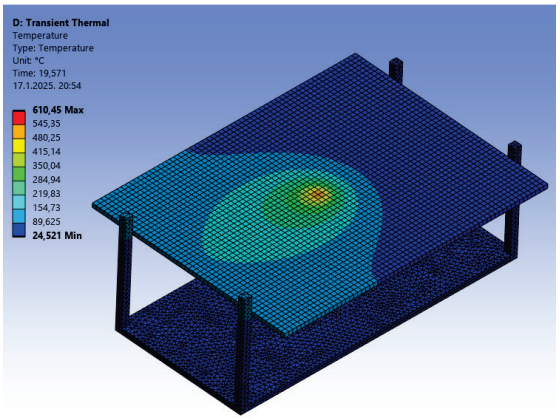

Figure 13 Temperature distribution in a 150 × 195 mm plate welding simulation

Fig. 14 presents the temperature distribution over time at measured points on the plate with dimensions of 150 × 195 mm.

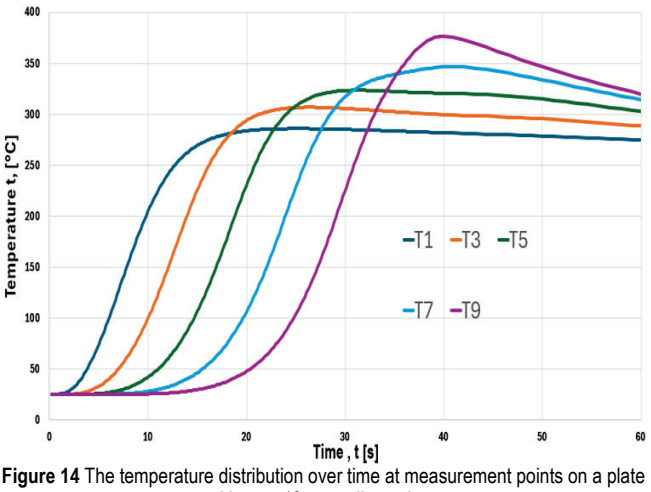

Figure 14 The temperature distribution over time at measurement points on a plate with 75 × 195 mm dimensions

The temperatures were measured using thermal probes in ANSYS at the exact locations where thermocouples were fixed in actual heat input during the experiment. The

temperature values reach their maximum at a certain point, after which a gradual cooling occurs. The highest temperature is recorded on Thermocouple 9, while the other thermocouples register progressively lower temperatures depending on their distance from the heat source. The characteristics of the graph show that the temperature cycles are similar, with a clear gradient toward the edges of the plate, which is expected due to heat dissipation. A smaller plate size allows for faster attainment of higher temperatures, and the temperature peaks are more pronounced due to the limited heat dissipation capacity compared to larger plates.
In the ANSYS simulation for the smaller plate, the maximum temperature reached within the temperature cycle of the thermal probe is T_{max} = 380.37 °C (Fig. 15) at thermal probe T9/T10. For the larger plate, the maximum temperature is also reached at thermal probe T9/T10. Still, it is T_{max}=188,51 °C (Fig. 14). By comparing the maximum temperatures measured in the experiment (smaller plate: T_{max} = 180.15 °C, larger plate: T_{max} = 390 °C) with the maximum temperatures obtained in the simulation, it can be concluded that the simulation agrees very well with the experimental values. The difference in maximum temperatures is expected due to hidden heat dissipation during the experiment, which was not accounted for in the simulation.

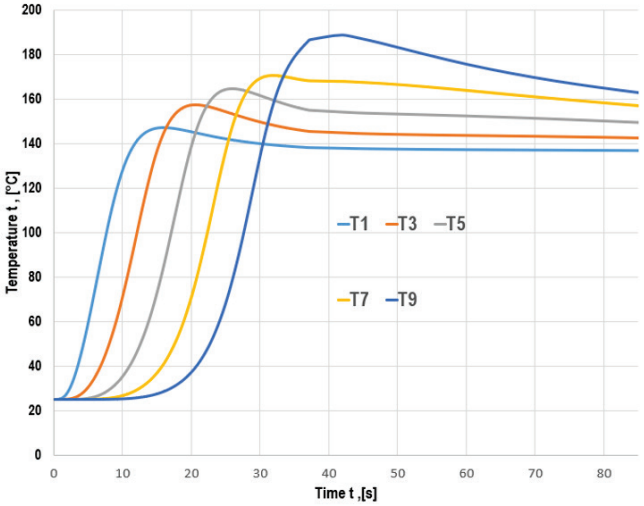

Figure 15 The temperature distribution over time at measurement points on a plate with 150 × 195 mm dimensions

5 CONCLUSIONS

This study confirmed the significant influence of copper plate dimensions on the temperature distribution during TIG welding. Experimental measurements and numerical simulations showed that smaller plates attain higher peak temperatures near the weld zone, while larger plates facilitate a more uniform heat distribution due to their increased heat dissipation capacity. It was also found that plate geometry and material properties strongly affect heat transfer dynamics: smaller plates exhibit steeper temperature gradients, whereas larger plates mitigate localized temperature peaks. Notably, the temperature gradient was approximately proportional to the plate dimensions.

Experimental results were consistent with the numerical simulations performed in ANSYS, with the discrepancy between measured and simulated temperatures remaining below 5%. This finding further corroborates the reliability of the employed methodology for analyzing thermal processes. The insights gained from this research are valuable for optimizing welding parameters and designing reliable joints in high thermal conductivity materials such as copper.

Future investigations could focus on a more detailed analysis of heat source distribution, allowing for more precise modeling and validation against experimental data. The heat source could be modeled according to Goldak's model [25] to more accurately represent heat flow. Additionally, implementing a finer computational mesh, particularly in the welding zone, should be considered in numerical simulations to achieve higher accuracy in local temperature gradients. These measures would further advance the understanding of thermal processes in TIG welding of copper.

Acknowledgements

This research was funded by: University North support for scientific research and artistic work in 2024 – UNIN-TEH-24-1-19.

6 REFERENCES

[1] Alfirević, I., Bjelovučić, D., Budin, I., Matijašević, B., Modlić, B., Mulc, A., Šikić, Z., & Taboršak, D. (1996). *Inženjerski priručnik IP 4 - Proizvodno strojarstvo, sv. 1 - Materijali*. Zagreb, Croatia: Školska knjiga. (in Croatian)
[2] American Welding Society. (1987). *Handbook for GTAW – Gas Tungsten Arc Welding*. Miami, FL: American Welding Society.
[3] American Welding Society. (2007). *Copper and alloys*. Miami, FL: American Welding Society.
[4] Rosenthal, D. (1946). The theory of moving source of heat and its application to metal transfer. *Transactions of the ASME, 43*, 849-866. https://doi.org/10.1115/1.4018624
[5] Christensen, N., Davies, V., & Gjermundsen, K. (1965). Distribution of temperatures in arc welding. *British Welding Journal, 12*, 54-75.
[6] Eagar, T. W., & Tsai, N. S. (1983). Temperature fields produced by traveling distributed heat sources. *Welding Journal, 62*, 346-355.
[7] Komanduri, R., & Hou, Z. B. (2000). Thermal analysis of the arc welding process: part I. General solutions. *Metallurgical and Materials Transactions B, 31*, 1353-1370. https://doi.org/10.1007/s11663-000-0022-2
[8] Nguyen, N. T., Ohta, A., Matsuoka, K., et al. (1999). Analytical solutions for transient temperature of a semi-infinite body subjected to 3-D moving heat sources. *Welding Research Supplement, I*, 265-274.
[9] Samardžić, I., Čikić, A., & Dunđer, M. (2015). Analytical heat conduction models at arc fusion welding. *Technical Gazette, 22*(6), 1641-1647. https://doi.org/10.17559/TV-20150220144751
[10] Ueda, Y., & Yamakawa, T. (1971). Analysis of thermal elastic-plastic stress and strain during welding by finite element method. *JWRI, 2*(2), 90-100.

[11] Hibbitt, H. D., & Marcal, P. V. (1973). A numerical, thermo-mechanical model for the welding and subsequent loading of a fabricated structure. *Computers & Structures, 3*, 1145-1174. https://doi.org/10.1016/0045-7949(73)90043-6
[12] Marcal, P. V. (1974). Weld problems. In *Structural Mechanics Computer Programs* (pp. 191-206). Charlottesville, VA: University Press.
[13] Goldak, J. A., Bibby, M., Moore, J., House, R., & Patel, B. (1986). Computer modelling of heat flow in welds. *Metallurgical Transactions B, 17B*, 587-600. https://doi.org/10.1007/BF02670226
[14] Karlsson, L. (1993). Thermomechanical finite element models for calculation of residual stresses due to welding. In Hauk, E. et al. (Eds.), *Residual Stresses* (p. 33). DGM Informationsgesellschaft Verlag.
[15] Lindgren, L.-E. (2001). Finite element modelling and simulation of welding – Part 1: Increased complexity. *Journal of Thermal Stresses, 24*, 141-192. https://doi.org/10.1080/01495730150500442
[16] Lindgren, L.-E. (2001). Finite element modeling and simulation of welding – Part 2: Improved material modeling. *Journal of Thermal Stresses, 24*, 195-231. https://doi.org/10.1080/014957301300006380
[17] Barac, A., Živić, M., Holik, M., Končić, R., & Samardžić, I. (2019). Comparison of experimental and analytical solutions of temperature field in a submerged arc welding. In *Engineering technologies in the manufacturing of welded constructions and products, SBW 2019*. Retrieved from https://dtzsb.unisb.hr/wp-content/uploads/radovi_2019/14_Zivic.pdf
[18] Fluke Corporation. (n.d.). *1586A Super-DAQ Precision Temperature Scanner*. Retrieved from https://www.fluke.com/en-us/product/calibration-tools/temperature-calibrators/fluke-calibration-1586a
[19] IEC 60584-1:2013. *Thermocouples – Part 1: EMF Specifications and Tolerances*.
[20] EURAMET Calibration Guide No. 11:2011. *Guidelines on the Calibration of Temperature Indicators and Simulators by Electrical Stimulation and Measurement*.
[21] Baker Hughes. (n.d.). *Premium temperature calibrators*. Retrieved from https://www.bakerhughes.com/druck/test-and-calibration-instrumentation/portable-pressure-temperature-calibrators-2/premium-temperature-calibrators
[22] Additel. (n.d.). *875 Dry well temperature calibrator*. Retrieved from https://additel.com/product-detail.html/875-dry-well-temperature-calibrator
[23] Bionda, F. (2018). *Automated TIG welding of stainless steel pipes* (Master's thesis). University of Zagreb, Faculty of Mechanical Engineering and Naval Architecture.
[24] Traidia, A. (2011). *Multiphysics modeling and numerical simulation of GTA weld pools* (Doctoral dissertation, Ecole Polytechnique X). (Published in English).
[25] Karkhin, V. A. (2019). *Thermal processes in welding*. Springer. https://doi.org/10.1007/978-981-13-5965-1

Authors' contacts:

Mihael Zelić, mag. ing. mech. & mag. educ. phys.
(Corresponding author)
Mačkovec, 40000 Čakovec, Croatia
E-mail: mihael.zelic@gmail.com

Matija Bušić, Assistant Professor
University North,
Ul. 104. Brigade 3, 42000 Varaždin, Croatia
E-mail: mbusic@unin.hr

Tomislav Veliki, Assistant Professor
University North,
Ul. 104. Brigade 3, 42000 Varaždin, Croatia
E-mail: tveliki@unin.hr